Received: 9 January 2017 | Revised: 6 June 2017 | Accepted: 29 August 2017

DOI: 10.1002/cta.2422

RESEARCH ARTICLE

WILEY

An oscillatory noise-shaped quantizer for time-based continuous-time sigma-delta modulators

Mohsen Tamaddon | Mohammad Yavari

Integrated Circuits Design Laboratory, Department of Electrical Engineering, Amirkabir University of Technology (Tehran Polytechnic), Tehran, Iran

Correspondence
Mohammad Yavari, Integrated Circuits Design Laboratory, Department of Electrical Engineering, Amirkabir University of Technology (Tehran Polytechnic), Tehran, Iran.
Email: myavari@aut.ac.ir

Summary

In this paper, a new type of an oscillatory noise-shaped quantizer (NSQ) for time-based continuous-time sigma-delta modulators is presented. The proposed NSQ is composed of an oscillatory voltage-to-time converter and a polyphase sampler. Using Tustin's transformation method and through the approximation of the comparator gain, a linearized model of the NSQ is introduced. This way, a novel realization of the first- and second-order NSQ is presented. Its implementation is based on fully passive continuous-time filters without needing any amplifier or power consuming element. The ploy-phase sampler inside the NSQ is based on the combination of a time-to-digital and a digital-to-time converter. The layout of the proposed NSQ is provided in Taiwan Semiconductor Manufacturing Company 0.18 μm complementary metal-oxide-semiconductor 1P6M technology. The verification of the proposed NSQ is done via investigating both the system level and postlayout simulation results. Leveraging the proposed NSQ in an Lth-order time-based continuous-time sigma-delta modulator enhances the noise-shaping order up to $L + 2$, confirming its superior effectiveness. This makes it possible to design high performance and wideband continuous-time SDMs with low power consumption and relaxed design complexity.

KEYWORDS

continuous-time sigma-delta modulators, describing function, noise-coupling, noise-shaped quantizer, time-based

1 | INTRODUCTION

Noise transfer function (NTF) enhancement through the noise-coupling (NC) is found to be an efficient method for increasing the noise-shaping order in sigma-delta modulators (SDMs). The concept has been well established for discrete-time (DT) SDMs.[1,2] However, it is not straightforward to apply this technique in continuous-time SDMs (CTSDMs).[3,4] The challenge gets more severe if higher order of NC is desired for single-bit CTSDMs. This is owing to the difficulty in implementing the analog subtractor, which is required to extract the quantization noise. In Wang and Temes,[3] a DT NC branch using a switched-capacitor circuit and a clocking scheme is utilized to realize the NC in a CT SDM. Although it is shown that the first-order NC is achieved, the introduced modulator is not fully continuous-time because the NC branch utilizes a DT active subtractor. This DT approach makes it an unsuitable choice for wideband and low power applications.

On the other hand, calculating the NTF is required to use the NC approach in conventional CTSDMs. Compared with the DT SDMs, it is a demanding task to calculate the NTF in CTSDMs.[5]

Some generalized approaches in the context of automated control systems have been already developed to introduce a semilinear model for the comparator-based closed-loop systems. Describing function (DF), the frequently used method, is a simple approach that can provide sufficiently accurate estimations of the frequency and amplitude of a possible periodic oscillation.[6-9] Hence, the DF theory can be regarded as an efficient method to calculate the NTF response in CTSDMs. However, the dependency of DF to the input signal amplitude complicates its usage in the analysis of CTSDMs.

If a comparator is located inside an oscillatory closed-loop system, its associated gain and phase can be calculated through the Barkhausen's criteria. In this case, the SDM works at the limit-cycle mode.[10-14] This way, a linearized model may be attributed to the SDM for the sake of a simple mathematical analysis. This makes it possible to develop a new method for applying the NC technique in CTSDMs. However, voltage-mode CTSDMs may not be benefited from this approach as they are not usually designed to work at the limit-cycle mode. In contrast, if the quantization is performed in time domain instead of the voltage mode, the associated time-based SDM can operate at both the clock[15,16] and limit-cycle modes.[17-19] For a time-based SDM working at the limit-cycle mode, the oscillation frequency f_c can be regarded as a counterpart of the clock frequency f_s (ie, $f_c < f_s$). This way, the nonlinearity problem of the comparator is resolved, making it possible to mathematically analyze the modulator.

Reported in Tamaddon and Yavari,[14,20] the NTF-enhanced TCSDMs realize the first- and second-order NC ideas, respectively. In these TCSDMs, the NC concept is implemented by taking advantage of the excess loop delay compensation branch. Thus, the operation of their quantizers depends on the whole TCSDM structure. It means that the quantizers are malfunctioned if they are taken apart from the TCSDM loop. This dependency makes it difficult to analyze both the TCSDM and the time-based quantizer. Thus, it is necessary to design an individual noise-shaped quantizer (NSQ) for use in NTF-enhanced TCSDMs.

In this paper, an oscillatory NSQ is proposed for time-based CTSDMs (TCSDMs). The noise-shaping in the NSQ is achieved through a novel implementation of the NC idea. The NSQ is designed to provide both the first- and second-order noise-shaping capabilities, thanks to the time-based quantization approach. This is achieved without using any extra amplifier. Also, the proposed NSQ utilizes a novel fully digital time-based polyphase sampler. This sampler resolves the need of a multibit digital-to-analog converter (DAC) if the proposed NSQ is targeted to be utilized in a TCSDM.

Although the concept of the NSQ was first introduced by Tamaddon and Yavari,[21] its performance and the detailed analysis are further elaborated in this paper. In Tamaddon and Yavari,[21] the reported CTSDM incorporates the NSQ to enhance its performance; however, the performance of the NSQ itself is not fully investigated. Hence, a detailed insight of the NSQ seems to be necessary to generalize the concept. For this target, a detailed elaboration is devoted for the proposed NSQ in this paper. Followed by the analytical approach, its performance is examined by using the extensive simulations. Furthermore, the layout of the NSQ is drawn in Taiwan Semiconductor Manufacturing Company 0.18 μm complementary metal-oxide-semiconductor (CMOS) technology, and the postlayout simulation results are given to confirm the performance of the NSQ. This way, a simple design method is accomplished that makes it possible to employ the proposed NSQ for any kind of the CTSDMs.

The paper is organized as follows. In Section 2, the asynchronous oscillatory voltage-to-time converter (VTC) is presented and the comparator gain approximation is analyzed. The proposed NSQ is introduced in Section 3. Section 4 presents a design example for the TCSDM, and its behavioral simulation results are also provided. Finally, the conclusions are given in Section 5.

2 | OSCILLATORY VOLTAGE-TO-TIME CONVERTER

2.1 | Asynchronous oscillatory voltage-to-time converter

The block diagram of an asynchronous oscillatory VTC is shown in Figure 1. Unlike the synchronous oscillatory VTC, the sampler is located outside the feedback loop. Excluding the sampler from the oscillatory loop makes it possible to break the dependency of the oscillation frequency to the sampler clock rate.[18] As a result, in the asynchronous VTC, the oscillation frequency depends only on the loop parameters, making it possible to design a robust time-based quantizer.[19]

The asynchronous oscillatory VTC is composed of a linear filtering block denoted by $A(s)$, a nonlinear element and a delay unit named as T_d. Denoting the zero-input oscillation frequency of the VTC with f_c, the sampling frequency f_Q, is

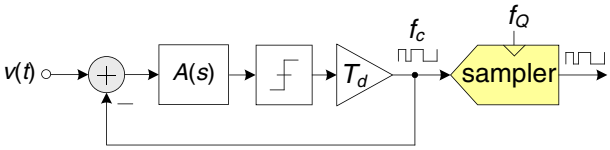

FIGURE 1 Block diagram of an asynchronous oscillatory voltage-to-time converter (VTC) [Colour figure can be viewed at wileyonlinelibrary.com]

much larger than f_c (ie, $f_Q \gg f_c$). Because the asynchronous oscillatory VTC is the starting point of the proposed NSQ, its analysis is given in the following.

Most of the reported oscillatory VTCs are implemented by using a hysteretic comparator preceded by an active integrator.[22-24] The typical implementation of this kind of VTC is shown in Figure 2A. In this topology, the maximum integrator output voltage is limited by the hysteresis factor, h. However, if a zero hysteresis comparator is utilized instead, the comparator input signal swing is not restricted by the hysteresis factor anymore. If the signal swing is larger than the comparator output level, it may cause the loop to be unstable. Thus, the integrator should be modified to prevent the saturation of the comparator. Scaling the coefficient of the integrator or realizing a nonzero pole for the integrator can be the alternatives for this issue. However, in the proposed NSQ, the oscillatory VTC is of another kind. As shown in Figure 2B, the active integrator is replaced with a mere summing amplifier. In the proposed VTC, the required phase shifting in the oscillatory loop is obtained by using a passive low-pass filter (LPF) denoted as $A(s) = \omega_a/(s + \omega_a)$, where

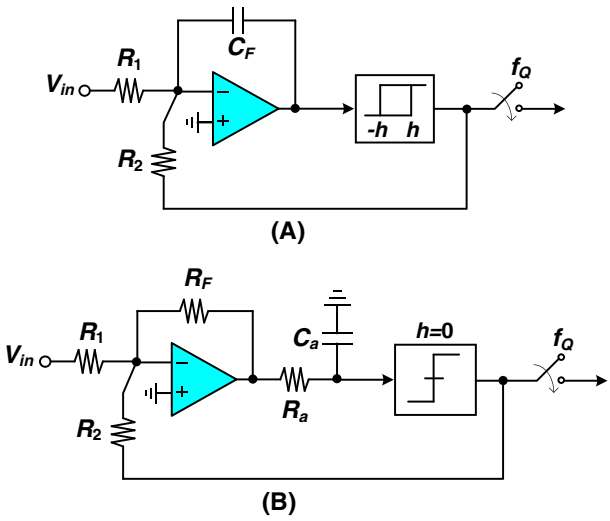

FIGURE 2 (A) Typical implementation of the frequently used oscillatory voltage-to-time converter (VTC) and (B) schematic of the proposed oscillatory VTC [Colour figure can be viewed at wileyonlinelibrary.com]

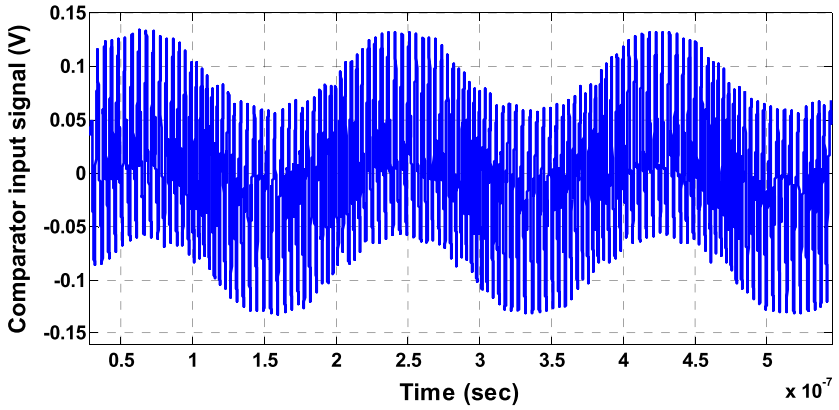

FIGURE 3 Simulation of the signal swing at the input of the comparator [Colour figure can be viewed at wileyonlinelibrary.com]

$\omega_a = 1/R_aC_a$. Using a passive LPF attenuates the comparator input signal swing to further improve the stability. On the other hand, using a summing amplifier instead of the front-end active integrator significantly reduces the internal signal swing, and thus, the stability is further improved. This feature is shown in Figure 3. As it is clear, the signal swing at the comparator input is much less than the Operational Transconductance Amplifier (OTA) full-scale rang. Furthermore, as will be shown in Section 3, replacing an active integrator with a summing amplifier in the proposed VTC offers a novel feasibility in the implementation of the proposed NSQ.

Although a little bit of the hysteresis in a binary comparator is unavoidable, it only affects the VTC feedforward path delay. Thus, it cannot be a critical problem in the proposed VTC. By trimming the value of T_d, the excess delay of the comparator, owing to its inherent hysteresis, is compensated.

2.2 | Oscillation analysis of the proposed voltage-to-time converter

Barkhausen's well-known gain-phase relations can be applied to analyze the oscillation of the proposed VTC. Applying the oscillation phase criterion for the VTC shown in Figure 1, it can be stated that

$$-\tan^{-1}(\omega_c/\omega_a) - \omega_c T_d - \pi = -2\pi \tag{1}$$

By solving Equation 1, the oscillation frequency, f_c, can be estimated as

$$f_c = \frac{1}{2\pi} \times \frac{\pi - \tan^{-1}(\omega_c/\omega_a)}{T_d} \approx \frac{1}{4T_d} \qquad @\,\omega_c >> \omega_a \tag{2}$$

Here, we assumed a zero-hysteresis binary comparator for the VTC nonlinearity. However, the oscillation gain criterion is also necessary to efficiently study the oscillatory VTC. For this, the comparator gain should be calculated. Assuming the binary comparator gain as k_{comp}, the oscillation gain relation can be given as

$$A(j\omega)E(j\omega) = -1/k_{\text{comp.}} \qquad @\,\omega = \omega_c \tag{3}$$

where $E(s) = e^{-sTd}$ represents the delay element of T_d. The crossing point between the Nyquist plot of $A(j\omega)E(j\omega)$ and the locus of $-1/k_{\text{comp}}$ shows the possible oscillation frequency notated as f_c. However, the gain of a binary comparator is an unknown value owning to its nonlinearity. Applying the DF technique to quasi linearly approximate the comparator gain can be a proper method to predict the possible oscillation modes of the VTC. Using DF technique, k_{comp} can be approximated as $k_{\text{DF}} = 4/m\pi$, where m is the primary component amplitude of the comparator input signal.[7] Furthermore, to linearly solve Equation 3, the nonlinearity of the transfer function attributed to the delay element should also be resolved. Thus, to extend the mathematical analysis of the VTC and subsequently the proposed NSQ, a linear representation for $E(s)$ is required.

There are some approximations that have rational polynomial forms for the delay element such as Forward Euler (*F.E*), Backward Euler (*B.E*), and Tustin's approximations as are stated in Equation 4:

$$E(s) \triangleq e^{-sT_d} \approx \begin{cases} 1 - sT_d & \text{Forward Euler approx.} \\ \dfrac{1}{(1+sT_d)} & \text{Backward Euler approx.} \\ \left(1 - \dfrac{sT_d}{2}\right) \Big/ \left(1 + \dfrac{sT_d}{2}\right) & \text{Tustin's approx} \end{cases} \tag{4}$$

Equation 3 is said to be appropriately solved if the resulting crossing point, f_c, has a negligible difference with the one calculated in Equation 2. This is achieved if an efficient representation is applied for the delay element. To study this, we examine Equation 3 through the behavioral simulations of the VTC with several representations of $E(s)$ and applying k_{DF} as for the k_{comp}. Then, the simulation results are compared with the previously calculated oscillation frequency in Equation 2. The Nyquist plots of Equation 3 are illustrated in Figure 4 for 3 different cases: $T_d = 0.2$ ns, 0.4 n, and 2 ns, which, according to Equation 2, are associated to $f_c = 1.25$ GHz, 625 MHz, and 125 MHz, respectively. The comparison results verify that predicting of f_c by graphically solving Equation 3 may have a negligible difference with Equation 2 if the Tustin's approximation is applied for the delay element. This confirms the validity of the Tustin's representation for

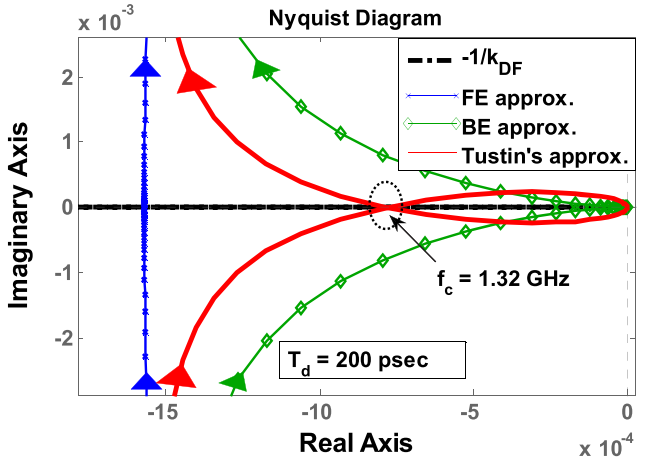

(A)

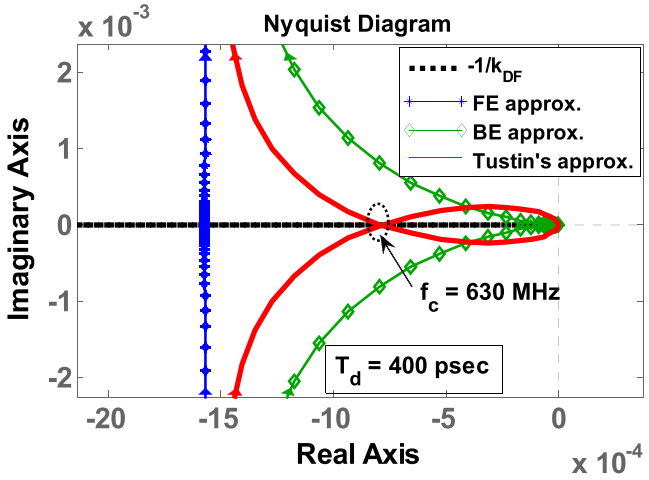

(B)

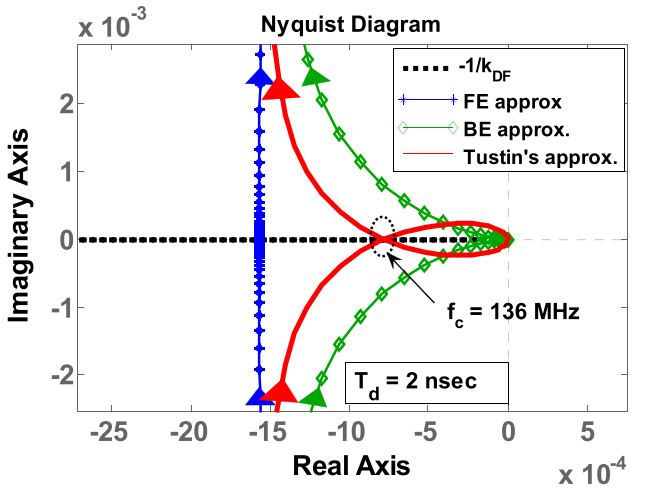

(C)

FIGURE 4 Graphical determination of the voltage-to-time converter (VTC) oscillation frequency for 3 different approximations of the delay element, (A) $T_d = 200$ ps, (B) $T_d = 400$ ps, and (C) $T_d = 2$ ns [Colour figure can be viewed at wileyonlinelibrary.com]

the linear analysis of the VTC and also the proposed NSQ. It should be noted that the accuracy of the Tustin's approximation for $E(s)$ holds if $\omega_c >> \omega_a$ as implied in Equation 2.

2.3 | Comparator gain approximation

As emphasized in the introduction, the main target is to explore a linearized model for the NSQ. However, using the DF method to overcome the nonlinearity of the comparator has a shortcoming. Although the graphical analysis approaches can take advantages of the DF technique, the dependency of the k_{DF} to the comparator input signal amplitude (m) makes it difficult to develop a general linear model for the VTC and the NSQ. In this section, we will calculate a new approximation for the comparator gain. This way, a generalized linear model will be developed for the proposed NSQ.

For an oscillatory VTC with the Tustin's representation for $E(s)$, the gain criterion at the oscillation frequency of ω_c can be applied to approximate the comparator gain as

$$\frac{\omega_a}{\sqrt{\omega^2+\omega_a^2}} \times \left|\frac{2-j\omega T_d}{2+j\omega T_d}\right| \times k_{app.} = 1 \qquad @\,\omega = \omega_c \tag{5}$$

From Equation 5, the approximated comparator gain is obtained as

$$k_{app.} = \sqrt{1+(\omega_c/\omega_a)^2} \tag{6}$$

As it is clear, k_{app} is a constant value and depends only on the ω_a and ω_c. However, its validity should also be evaluated in comparison with the frequently used methods to model the comparator's nonlinearities. Describing function model is utilized for this target due to its higher accuracy (ie, $k_{DF} = 4/m\pi$). Time consuming Fourier series analysis is usually utilized to determine the amplitude, m. When the difference between k_{DF} and k_{app} is small, an accurate model for the comparator is achieved. The associated error percentage assumed as $1-(k_{app}/k_{DF})$ is plotted versus the VTC input signal amplitude in Figure 5, where $R = \omega_c/\omega_a$.

As it is clear, the validity of k_{app} is more satisfied if $\omega_c \gg \omega_a$ (ie, $\omega_c > 10\omega_a$). It is worth mentioning that the proposed linear approximation of the comparator gain is accessible because it is located inside an oscillatory loop. Otherwise, the determination of the comparator gain in the conventional voltage-mode quantizers is not a straightforward task.

3 | PROPOSED NOISE-SHAPED QUANTIZER

3.1 | Noise-shaping concept

An NTF enhancement through the NC is an interesting technique to increase the noise-shaping performance of an SDM. In this technique, the quantization noise of the quantizer is extracted by using a subtractor. Then, the error is passed through an FIR filter $G(z)$ and injected to the quantizer input again. It is proven in Lee et al and Wang and Temes[1-3] that by using this technique, the new NTF is enhanced as $(1-G(z)) \times \mathrm{NTF}_{old}$. Although it is difficult to take advantage of this

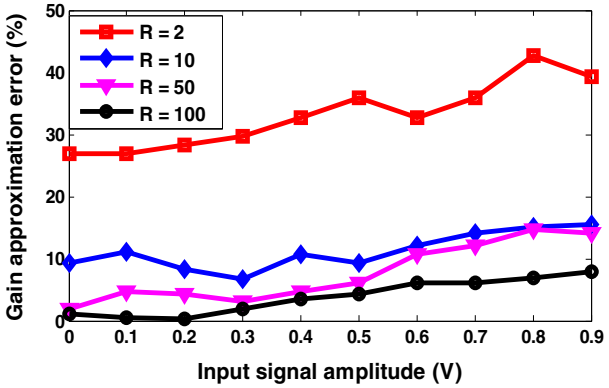

FIGURE 5 The error associated to the approximated comparator gain, $R = \omega_c/\omega_a$ [Colour figure can be viewed at wileyonlinelibrary.com]

idea in the conventional CTSDMs,[14,20] in this paper, a new approach is introduced for this technique to make it applicable to the proposed time-based quantizer.

Successfully developing the linearized model of the oscillatory VTC, the proposed continuous-time NSQ can be organized by applying the NC idea introduced in Lee et al[1] to the VTC. Obviously, some necessary modifications may be required. The simplified block diagram of the NSQ is shown in Figure 6A. The $G(s)$ block is a continuous-time transfer function. The extended version of the NSQ is also depicted in Figure 6B. By merging the VTC feedback branch with the inner $G(s)$, the NSQ gets more simplified. Its finalized version is illustrated in Figure 6C.

Realization of the proposed NSQ is feasible if a proper transfer function is determined for $G(s)$. This is calculated according to the NTF of the NSQ. For this target, the transfer function of the sampler is required. The time-based sampler performs a sample and hold operation with the sampling frequency of f_Q. The associated frequency response of this operation is given by

$$H_{\text{sampler}}(s) = \text{sinc}\left(\frac{f}{f_Q}\right) \tag{7}$$

For $f \ll f_Q$, which is usually the case in SDMs, the magnitude of $\text{sinc}(f/f_Q)$ is assumed as 1.

As a consequence, the linearized signal flow graph of the NSQ is shown in Figure 6D, where E_Q denotes the quantization error.

According to the signal flow graph, the closed-loop transfer function of the proposed NSQ denoted by $H_{\text{CL}}(s)$ can be calculated as

$$H_{\text{CL}}(s) = \frac{\left(\frac{A(j\omega)E(j\omega)k_{\text{app.}}}{1+(1-G(j\omega))A(j\omega)E(j\omega)k_{\text{app.}}} \times 1\right) G(j\omega)}{1+\left(\frac{A(j\omega)E(j\omega)k_{\text{app.}}}{1+(1-G(j\omega))A(j\omega)E(j\omega)k_{\text{app.}}} \times 1\right) G(j\omega)} \tag{8}$$

Considering Equation 8, the NSQ oscillates if

$$\left(\frac{A(j\omega)E(j\omega)k_{\text{app.}}}{1+(1-G(j\omega))A(j\omega)E(j\omega)k_{\text{app.}}}\right) G(j\omega) = -1 \;\; @\,\omega = \omega_c \tag{9}$$

By rearranging Equation 9, it can be shown that

$$A(j\omega)E(j\omega) = -1/k_{\text{app.}} @\,\omega = \omega_c \tag{10}$$

From Equation 10, it is concluded that the oscillation criteria of the NSQ are the same as the oscillatory VTC and are independent of $G(s)$. Thus, the NTF of the NSQ is calculated as

$$\text{NTF}(s) = \frac{1}{1+\left\{\frac{G(s)A(s)E(s)k_{\text{app.}}}{1+(1-G(s))A(s)E(s)k_{\text{app.}}}\right\}} \tag{11}$$

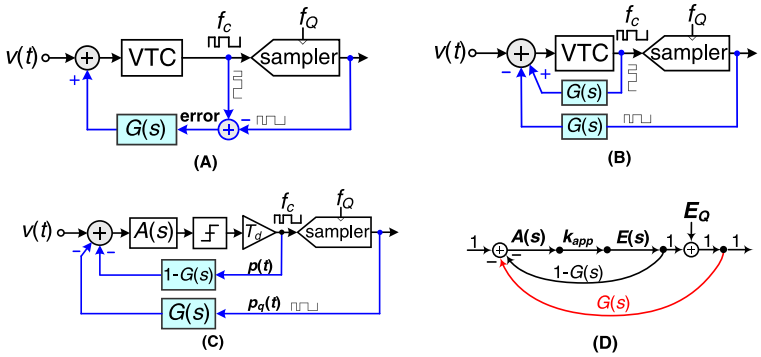

FIGURE 6 Noise-shaped quantizer (NSQ) block diagram, (A) its concept, (B) the extended version, (C) the finalized model, and (D) its linearized signal flow graph (SFG) [Colour figure can be viewed at wileyonlinelibrary.com]

Recalling the conventional SDMs, the frequency response of $NTF(s)$ in Equation 10 should have a high-pass profile. For this to be true, the term inside the bracket should act as an LPF such as $T_{\mathrm{LPF}}(s)$. This way, $G(s)$ can be calculated as

$$G(s) = \left\{\frac{1 + A(s)E(s)k_{\mathrm{app.}}}{A(s)E(s)k_{\mathrm{app.}}}\right\} \times \frac{T_{\mathrm{LPF}}(s)}{1 + T_{\mathrm{LPF}}(s)} \tag{12}$$

For sufficiently large values of comparator gain, k_{app}, the first term of Equation 12 can be simplified as ≈1. Hence, the approximated representation of $G(s)$ can be stated as

$$G(s) \approx \frac{T_{\mathrm{LPF}}(s)}{1 + T_{\mathrm{LPF}}(s)} \tag{13}$$

Recalling the well-known approach in designing the DT SDMs, z-domain analysis may be an efficient method to estimate $T_{\mathrm{LPF}}(s)$. Let us represent $T_{\mathrm{LPF}}(s)$ as $T_{\mathrm{LPF}}(z)$ in DT domain. Noting that $T_{\mathrm{LPF}}(z)$ is a DT LPF, we can use the Tustin's function of the "*d2c*" command in MATLAB® to calculate $T_{\mathrm{LPF}}(s)$. By applying the results in Equation 13, the functions $G(s)$ and $F(s)$ can be calculated. The normalized results are given in Table 1, where $F(s) = 1 - G(s)$.

TABLE 1 Calculation of the Tustin's representation of $G(s)$ and $F(s)$ [Colour table can be viewed at wileyonlinelibrary.com]

NSQ Order (L_{NS})	$T_{\mathrm{LPF}}(z)$	$G(s)$	$F(s)$
$L_{\mathrm{NS}} = 1$	$\frac{1}{1 - z^{-1}}$	$\frac{0.34s + 0.67}{s + 0.67}$	$\frac{0.67s}{s + 0.67}$
$L_{\mathrm{NS}} = 2$	$\frac{1}{(1 - z^{-1})^2}$	$\frac{0.2s^2 + 0.8s + 0.8}{s^2 + 0.8s + 0.8}$	$\frac{0.8s^2}{s^2 + 0.8s + 0.8}$

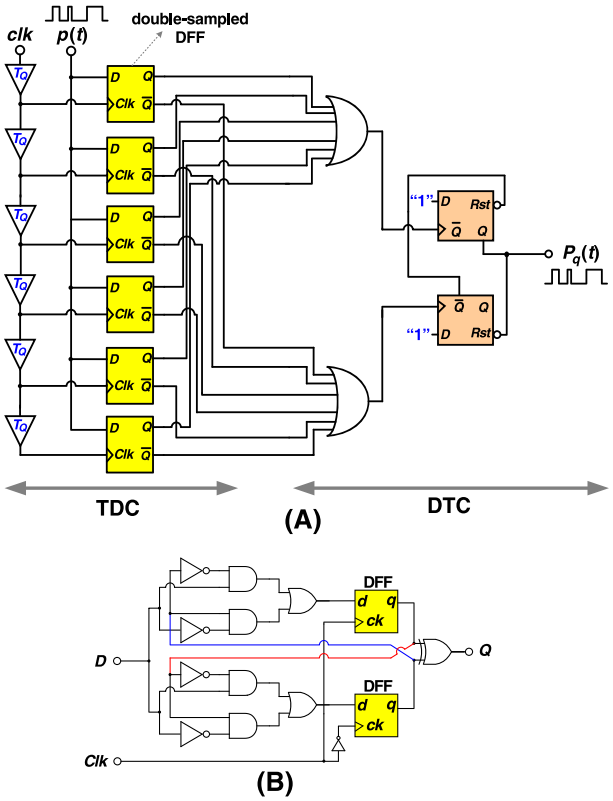

FIGURE 7 (A) The proposed polyphase sampler combined of a time-to-digital converter (TDC) and a digital-to-time converter (DTC) for N = 6 and (B) the behavioral modeling of a double-sampled D-flip flop [Colour figure can be viewed at wileyonlinelibrary.com]

For denormalization of the Tustin functions given in Table 1, one can replace s with sT, where $T = 1/f_c$ is the period of the NSQ oscillation. Hence, T determines the time constant of the Tustin's functions.

3.2 | The polyphase sampler

For an oscillatory VTC, for the proper detection of the pulse edges, the minimum required sampling frequency, f_Q, should be at least 4 times of f_c.[20] This important constraint is difficult to be satisfied in wideband TCSDMs. A polyphase sampler can be a suitable alternative to relax this severe constraint.[20] The polyphase sampler, shown in Figure 7A, is composed of an N-stage time-to-digital converter (TDC) followed by a digital-to-time converter (DTC). The resolution of the TDC is T_Q (ie, $T_Q = 1/f_Q$). The TDC is clocked at the rate of f_s, where $f_s = f_Q/N$. Applying a double-sampled DFFs in the TDC gives the possibility of reducing f_s as $f_s = f_Q/2\ N$.[14] The behavioral schematic of the double-sampled DFF is shown in Figure 7B. It is composed of 2 conventional DFFs each of them preceded by a multiplexer and an XOR gate, which merges the outputs of the DFFs. However, its real circuit implementation can be realized by using several digital logic gates to decrease the complexity.[20] A merged structure of TDC/DTC receives the input signal, $p(t)$, and outputs its quantized version as $p_q(t)$. The associated time quantization error is denoted by E_Q. Having N stages in the TDC, the output of the polyphase sampler is still a single-bit stream. This makes it possible to resolve the need of a multibit DAC at the feedback path.

3.3 | System-level simulation of the proposed noise-shaped quantizer

To verify the effectiveness of the proposed NSQ, a system-level simulation of the structure shown in Figure 6C is provided by using MATLAB. The power spectral density (PSD) of the NSQ for different orders of the noise-shaping (L_{NS}) applying Hanning window is illustrated in Figure 8. As is clear, the proposed NSQ is capable in achieving first- and second-order noise-shaping provided that a proper transfer function is determined for $G(s)$.

To study the robustness of the proposed NSQ against the RC-product variations in the Tustin's functions, the time constant, T, is randomly varied as $T + \Delta T$. Here, a zero-mean Gaussian distribution with the standard deviation of $\sigma = 0.3\ T$ (ie, $T = 1/f_c$) is considered for ΔT. The histogram of the SNDR variations for 100 iterations is illustrated in Figure 9. In these simulation results, the input $V(t)$ is a -1 dBFS, 4.5 MHz sinusoidal signal. The oscillation frequency, f_c, is 550 MHz and ω_c/ω_a is 200. Also the sampler is based on the double-sampled DFFs, and the resolution of the TDC is $T_Q = 80$ ps.

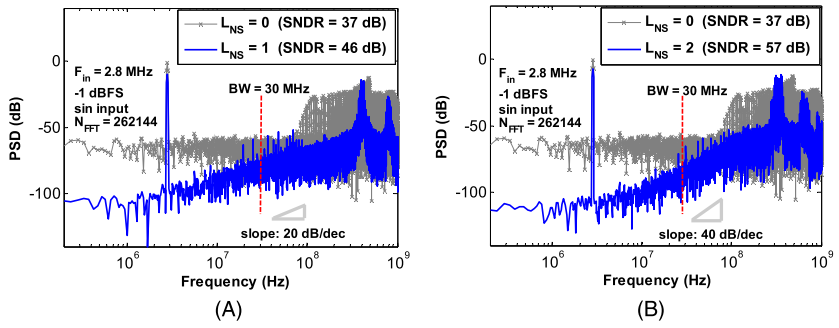

FIGURE 8 Simulated power spectral density (PSD) of the proposed noise-shaped quantizer (NSQ), (A) $L_{NS} = 1$, and (B) $L_{NS} = 2$ [Colour figure can be viewed at wileyonlinelibrary.com]

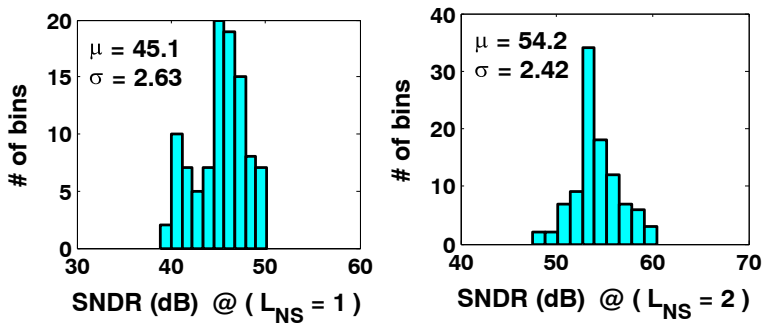

FIGURE 9 Performance of the noise-shaped quantizer (NSQ) versus the time constant variations [Colour figure can be viewed at wileyonlinelibrary.com]

As it is clear, the proposed NSQ has an acceptable degree of the robustness. This is achieved because in the proposed asynchronous VTC, the oscillation frequency depends only on the loop parameters and not on the predetermined clock frequency. Thus, the Tustin's functions are synthesized regarding the rate of the oscillation frequency and not according to the clock rate. If for any reason, the oscillation frequency is deviated from its defined value, the position of the poles and zeros of the functions are slightly changed. But, as long as $f_c \ll f_Q$, the NTF responses are not significantly changed. As a result, the performance of the NSQ is not severely deteriorated. To show the robustness of the NTF responses across the time constant variations of the Tustin's functions, the NTF Bode diagrams for $L_{NS} = 1$ and $L_{NS} = 2$ are provided in Figure 10. In these simulations, the time constant (ie, $T = 1/f_c$) of the Tustin's functions is randomly varied with the same distribution associated with Figure 9. According to Equations 12 and 13, the proposed NSQ can show a noise shaping performance if the NTF frequency response is a high pass profile. The slope of the NTF frequency response refers to the shaping degree of the NSQ. As is illustrated in Figure 10, the NTF of the NSQ for $L_{NS} = 1$ and $L_{NS} = 2$ are still a high pass profile with to some extent the same slope and cut-off frequency, even with a significant alteration in the Tustin's functions time constants.

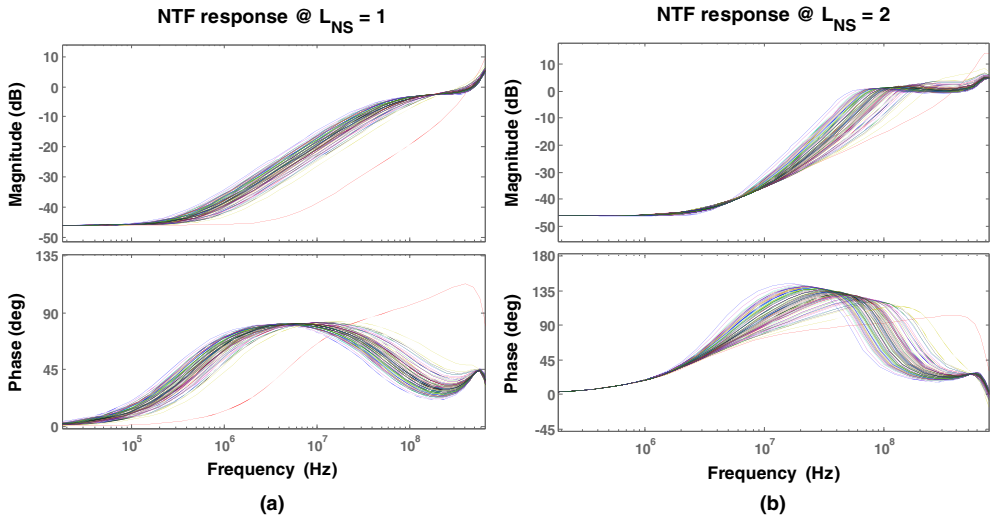

FIGURE 10 Noise transfer function (NTF) responses of the proposed noise-shaped quantizer (NSQ) against the time constant variations in the Tustin's functions, (A) $L_{NS} = 1$, and (B) $L_{NS} = 2$ [Colour figure can be viewed at wileyonlinelibrary.com]

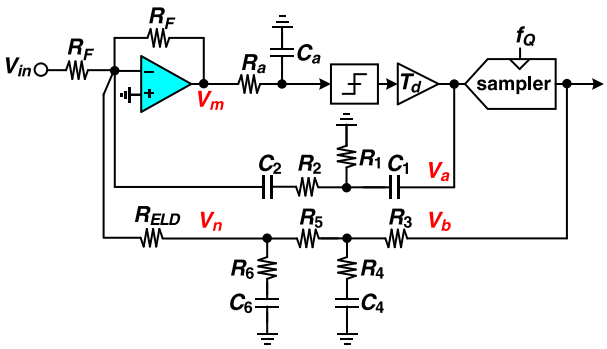

R_F	5 kΩ	R_2	5.5 kΩ	R_5	500 Ω	C_a	1.6 pF	C_4	0.3 pF
R_a	5 kΩ	R_3	1 kΩ	R_6	1 kΩ	C_1	18 pF	C_6	1 pF
R_1	50 Ω	R_4	1 kΩ	R_{ELD}	2.5 kΩ	C_2	0.3 pF		

FIGURE 11 Implementation of the proposed noise-shaped quantizer (NSQ) for $L_{NS} = 2$ [Colour figure can be viewed at wileyonlinelibrary.com]

3.4 | Implementation of the Tustin's functions

The proposed NSQ can be regarded as an efficient technique, if its implementation is a feasible task. A novel realization of the proposed NSQ according to the calculated Tustin's functions is introduced. In the conventional oscillatory VTCs, an active integrator is usually employed to enclose the feedback loop.[19] In contrast, as mentioned before, in the proposed NSQ, all of the feedback branches are collected by a unique summing amplifier. This way, as shown in Figure 11, the second-order Tustin's functions can be implemented just by using fully passive elements. So, there is no need to an extra amplifier for this target. The transfer function V_m/V_a refers to the second-order $F(s)$, while V_n/V_b realizes the second-order $G(s)$. Here, the damping factor of the $G(s)$ is determined to be about 1 (ie, $\xi \approx 1$). This way, the Tustin's functions can be realized by using cascaded RC ladders. Fortunately, this slight modification does not have a significant effect on the NSQ performance.

Because the implementation of the first-order Tustin's function is not a challenging task, its implementation is not covered for the sake of briefness. It should be mentioned that the realization of NSQs with $L_{NS} > 2$ is conceptually feasible. However, their implementation is not fulfilled with a mere summing amplifier and more active elements may be needed.

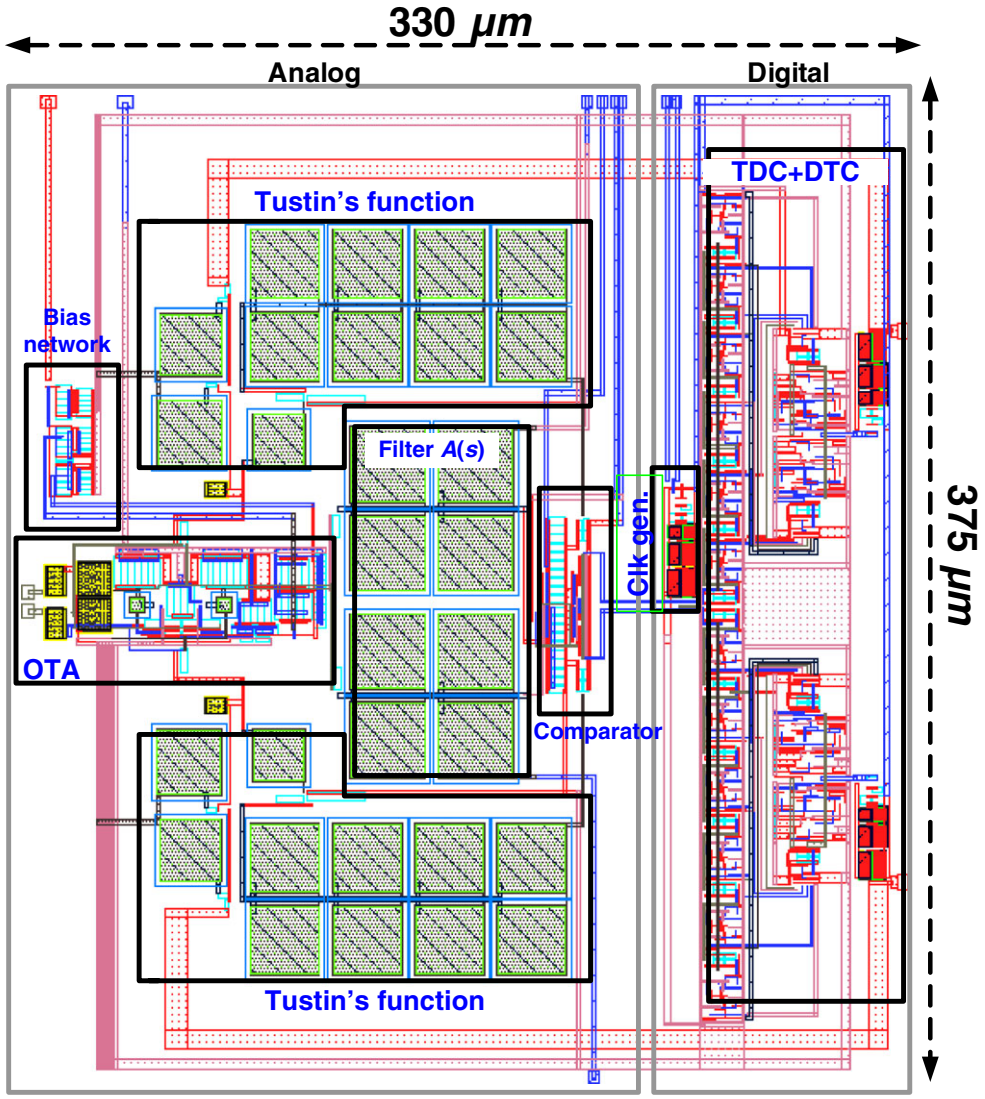

FIGURE 12 Layout of the proposed noise-shaped quantizer (NSQ) for $L_{NS} = 2$ drawn in Taiwan Semiconductor Manufacturing Company (TSMC) complementary metal-oxide-semiconductor (CMOS) 0.18 μM technology [Colour figure can be viewed at wileyonlinelibrary.com]

3.5 | Verification of the proposed noise-shaped quantizer

The signal-to-noise ratio (SNR) within the signal bandwidth of f_{BW} for the TCSDM has been previously developed in Tamaddon and Yavari[14] as

$$\mathrm{SNR} \simeq \frac{3}{8}U_p^2(L_{\mathrm{eff}}-0.5)^2\frac{2L_{\mathrm{eff}}+1}{\pi^{2L_{\mathrm{eff}}}}\left(\frac{f_Q}{f_c}\right)^2 \mathrm{OCR}^{2L_{\mathrm{eff}}+1} \tag{14}$$

where U_p is the input signal amplitude, L_{eff} is the effective noise-shaping order, and OCR is the overcycling ratio defined as $f_c/2f_{BW}$. The proposed NSQ can be conceived as a time-based sub-ADC with the shaping order of L_{NS}. Consequently, relation 14 can also be applied to predict the SNR of the proposed NSQ by choosing $L_{\mathrm{eff}} = L_{NS}$. Theoretically, by applying the parameters considered in the previous section and using Equation 13, the proposed NSQ with $L_{NS} = 2$ is capable in enhancing the SNR about 28 dB compared with $L_{NS} = 0$. It is worth mentioning that the structure of the NSQ with $L_{NS} = 0$ is as the oscillatory VTC that is shown in Figure 2B. This means that for $L_{NS} = 0$, the polyphase sampler is located outside the feedback loop.

Although this improvement is observed regarding the system-level simulation results in the previous section, to better verify the performance of the proposed NSQ, its required circuits have been designed and the postlayout simulation results are provided.

Noise-shaped quantizer circuit design has been performed in Taiwan Semiconductor Manufacturing Company 0.18 μm CMOS 1P6M technology with 1.8 V supply voltage. The layout of the implemented differential NSQ with $L_{NS} = 2$ is shown in Figure 12. As it is seen, the occupied area excluding the pads and guard rings is about 330 × 375 μm. In this prototype, for the summing amplifier that is located at the front-end, a 2-stage Miller-compensated CMOS opamp is utilized. Also, for the comparator, a conventional differential cross-coupled common-source amplifier is employed, and for the sampler, the previously introduced polyphase sampler is implemented by using D-flip flops based on the TSPC logic.[20]

Applying the same design parameters used in the previous section, the PSD of the proposed NSQ for $L_{NS} = 0$ and $L_{NS} = 2$ applying Hanning window is shown in Figure 13. Also, the simulated SNDR versus the input signal amplitude is depicted in Figure 14. The total power dissipation of the NSQ is about 11 and 14 mW for $L_{NS} = 0$ and $L_{NS} = 2$, respectively. It should be noted that the main target is showing the significant performance improvement of the NSQ with $L_{NS} = 2$ compared with $L_{NS} = 0$. Thus, emphasizing the comparative amount of the SNDR enhancement is much more beneficial than the SNDR absolute values. As it is clear, the peak SNDR of the NSQ with $L_{NS} = 2$ is almost 19 dB higher than the NSQ with $L_{NS} = 0$. This achievement validates the effectiveness of the proposed NSQ performance.

As the oscillation frequency of the loop depends on the loop delay, the robustness of the comparator delay time against the process and mismatch variations is investigated by applying the circuit level Monte-Carlo simulation. In this examination, the transistor dimensions are varied based on the Gaussian distribution with the standard deviation of 5%. The result is shown in Figure 15 where the histogram of the comparator delay variations regarding to the nominal one is illustrated for 100 iterations.

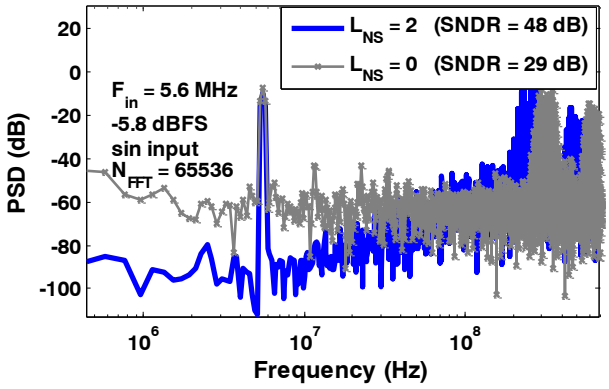

FIGURE 13 Post layout simulated power spectral density (PSD) of the proposed noise-shaped quantizer (NSQ) [Colour figure can be viewed at wileyonlinelibrary.com]

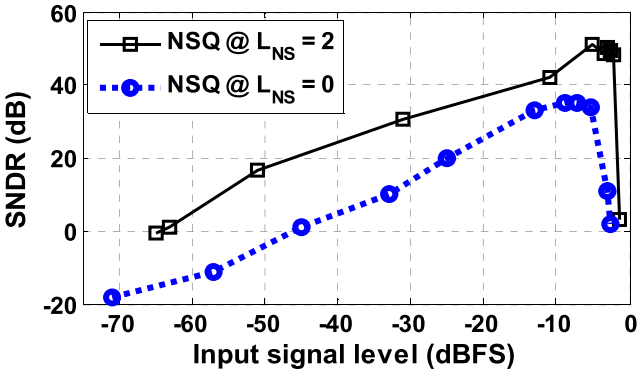

FIGURE 14 Postlayout simulated signal-to-noise and distortion ratio versus the input signal amplitude in the proposed noise-shaped quantizer (NSQ) [Colour figure can be viewed at wileyonlinelibrary.com]

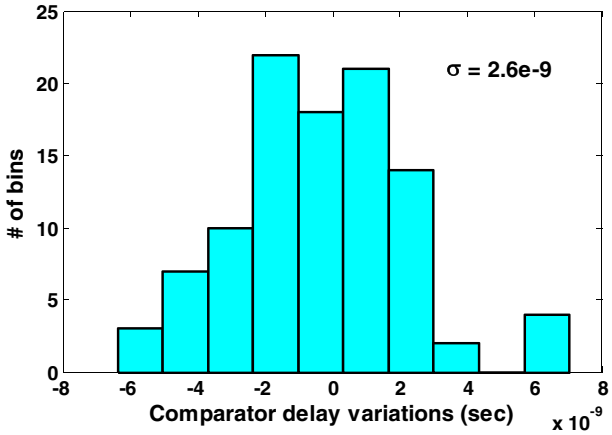

FIGURE 15 Monte Carlo simulation result of the comparator [Colour figure can be viewed at wileyonlinelibrary.com]

Although a passive loop filter is incorporated in the proposed NSQ structure, the noise shaping capability is achieved due to using the Tustin's functions. Despite the performance of the proposed NSQ is not comparable with high performance SDMs, it should be noted that the proposed NSQ is assumed to be utilized as a sub-ADC and not an individual modulator. Using it within the loop of a classical SDM will significantly enhance the performance of this modulator. This superiority is examined in section 4. The performance summary of the proposed NSQ for $L_{NS} = 1$ and $L_{NS} = 2$ is given in Table 2.

4 | DESIGN EXAMPLE FOR THE TIME-BASED CONTINUOUS-TIME SIGMA-DELTA MODULATOR

The proposed NSQ may be employed as a time-based quantizer in TCSDMs as shown in Figure 16. This way, the noise-shaping order of the TCSDM is increased by 1 or 2 regarding the order of the NSQ, L_{NS}. The modulator's loop filter is denoted with $H(s)$. The passive LPF represented as $L_f(s) = \omega_f/(s + \omega_f)$ is employed in the feedback path to suppress the high-frequency tones of $p_q(t)$ before being injected into the feedforward path. This is required because the high-frequency tones may destabilize the oscillatory VTC. Furthermore, $L_f(s)$ decreases the modulator's sensitivity to the clock jitter.

According to Equation 13, and assuming $L_{eff} = L + L_{NS}$ for a TCSDM with $L = 2$ and $OCR = 8$, the SNR improvement is about 36 dB if a second-order NSQ is utilized. This superiority is achieved by using only passive elements.

To make sure of the proposed TCSDM stability regarding the introduced linear model, the calculation of the NTFs seems to be necessary. With the values of the parameters given in Figure 16 and using the "*minreal*" function in

TABLE 2 The summary of the proposed NSQ performance [Colour table can be viewed at wileyonlinelibrary.com]

NSQ Type	Technology	V_{DD}	P_{diss} (mW)	N_{FFT}	SNDR (dB) (Prelayout)	SNDR (dB) (Postlayout)	Core Area (mm^2)
$L_{NS} = 1$	TSMC 0.18 μm CMOS	1.8 V	11	65,536	43	41	0.12
$L_{NS} = 2$	TSMC 0.18 μm CMOS	1.8 V	14	65,536	51	48	0.12

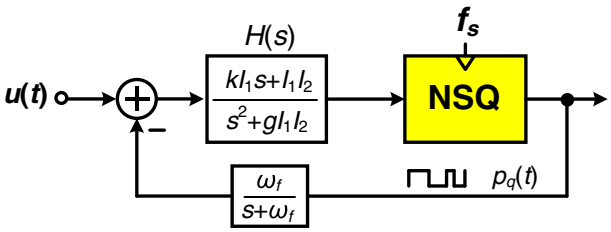

g	0.1	f_c (MHz)	550
I_1	3.8×10^8	f_s (GHz)	1
I_2	8.4×10^8	T_Q (psec)	80
k	1	T_d (psec)	375
ω_f (Mrad/sec)	2π×80	ω_c/ω_a	200

FIGURE 16 The block diagram of employing the proposed noise-shaped quantizer (NSQ) in a time-based continuous-time sigma-delta modulator (TCSDM) [Colour figure can be viewed at wileyonlinelibrary.com]

MATLAB®, the NTFs of the proposed TCSDM with $L = 2$ can be calculated for both $L_{NS} = 1$ and $L_{NS} = 2$ in Equations 14 and 15, respectively, as

$$\mathrm{NTF}(s) = \frac{s^3 + 3.312 \times 10^9 s^2 + 1.62 \times 10^{19} s + 9.38 \times 10^{25}}{s^3 + 2.068 \times 10^9 s^2 + 2.106 \times 10^{19} s + 9.477 \times 10^{27}} \quad @\, L_{NS} = 1 \tag{15}$$

$$\mathrm{NTF}(s) = \frac{s^4 + 2.89 \times 10^9 s^3 + 1.95 \times 10^{19} s^2 + 2.017 \times 10^{27} s + 7.15 \times 10^{34}}{s^4 + 2.134 \times 10^9 s^3 + 2.152 \times 10^{19} s^2 + 1.14 \times 10^{28} s + 7.22 \times 10^{36}} \quad @\, L_{NS} = 2 \tag{16}$$

The pole/zero maps of the calculated NTFs are also given in Figure 17. As it is clear, all of the poles and zeros are located in the left half plane, confirming the stability of the proposed TCSDM.[25] The following system-level simulation results also validate the stability of the proposed TCSDM regarding the introduced linear model.

The simulated PSD of the TCSDM with the parameters given in Figure 16 using Hanning window is illustrated in Figure 18. In this simulation, the main circuit nonidealities of the integrators and the summing amplifier are taken into account. The dc gain and unity gain bandwidth of the both utilized amplifiers in the modulator's loop filter are 40 dB and 1 GHz, respectively. For the summing amplifier at the NSQ front-end, the dc gain is 25 dB, while its UGBW is 2.5 GHz. Also, the limited swing and slew rate of the amplifiers are considered in the simulations.

Although the conventional CTSDMs are sensitive to the clock jitter, the proposed TCSDM shows a good robustness against this bottleneck. The clock signal is applied only at the sampler, which is located in the feedforward path. As a result, the clock jitter error is shaped similar to the quantization error. On the other hand, because the TDC outputs are merged by a DTC, some jitter rejection may be expected. In other words, because both the rising and falling edges of the feedback pulse denoted as $p_q(t)$ carry approximately the same time shift due to the clock jitter, it affects only the position of the feedback pulse and the pulse width remains approximately unchanged.[8]

However, the variation of the pulse edges of the feedback signal, $p_q(t)$ may deteriorate the TCSDM performance. This variation can be regarded as the clock jitter error existing in conventional CTSDMs. To show the performance of the proposed TCSDM in the presence of this error, the variation of $p_q(t)$ pulse width is modeled as an additive Gaussian white

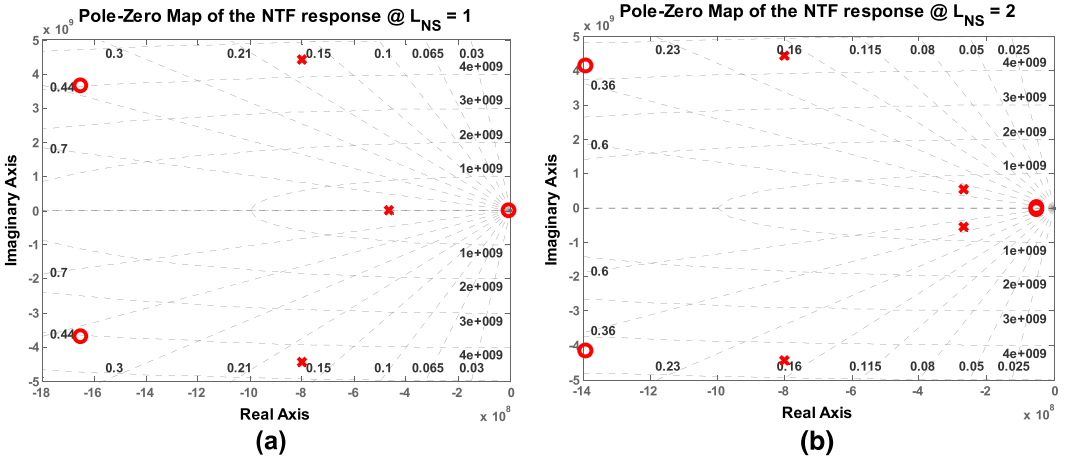

FIGURE 17 Poles and zeros locus of the proposed time-based continuous-time sigma-delta modulator (TCSDM) for $L = 2$, (A) $L_{NS} = 1$, and (B) $L_{NS} = 2$ [Colour figure can be viewed at wileyonlinelibrary.com]

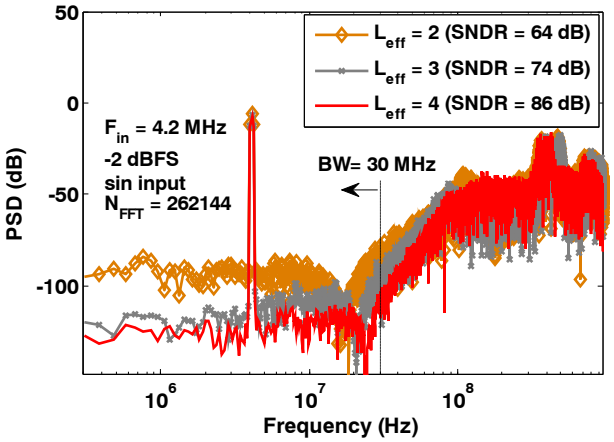

FIGURE 18 Simulated power spectral density (PSD) of the proposed noise-shaped quantizer (NSQ)-based time-based continuous-time sigma-delta modulator (TCSDM) with $L = 2$ [Colour figure can be viewed at wileyonlinelibrary.com]

noise as introduced in Ashry and Aboushady.[26] The result in Figure 19 confirms an acceptable robustness against the variation in the pulse width.

All of the results shown for the NSQ-based TCSDM are obtained by using the system-level simulations by considering the main circuit nonidealities. To compare the effectiveness of the proposed modulator, Table 3 highlights the main features of this work. Because the novelty of the paper is the NSQ, the postlayout simulation results are provided only for the proposed NSQ. However, to make the comparison a meaningful task, we need to compare the performance of the NSQ-based TCSDM rather than the NSQ itself. The aim is just to emphasize the advantages of incorporating the

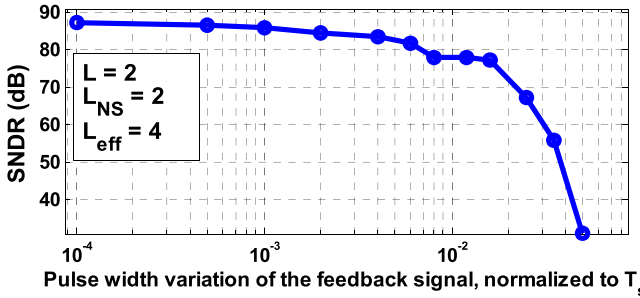

FIGURE 19 SNDR of the NSQ-based TCSDM versus the feedback pulse width variations [Colour figure can be viewed at wileyonlinelibrary.com]

TABLE 3 Proposed NSQ-based TCSDM performance comparison with other CT sigma-delta modulators [Colour table can be viewed at wileyonlinelibrary.com]

	# of Active Integrators	Noise Shaping Order (L)	Oscillation Frequency (MHz)	Clock Rate (GHz)	BW (MHz)	SNDR (dB)
[14]*	2	1	37.5	0.3	1.2	60
[16]*	2	2	106.25	0.85	5	56.1
[17]**	2	2	125	1	5	64
[27]*	3	3	250	250	20	60
[28]*	3	3	2560	2560	20	61
[29]**	3	3	1000	1000	10	43
This work**	2	4	550	1.04	30	86

*Measurement results.

**Simulation results.

proposed NSQ in the classical SDM. Hence, to have a fair comparison, we avoid using the figure-of-merit (FoM) in the comparison table.

As a comparison, the fabricated third-order CT SDM in Dhanasekaran et al[27] is considered. It employs a synchronous PWM and a delay-line-based 4-bit TDC with $N = 50$. It consumes 10.5 mW power from a 1.2 V power supply at 250 MHz sampling frequency and achieves 60 dB SNDR in 20 MHz bandwidth. The reported figure of merit (FoM = Power/$2 \times \text{BW} \times 2^{\text{ENOB}}$) is 319 fJ/conversion-step. Although this small FoM shows the superiority of this work over the comparable voltage-mode CT SDMs, the power consumption is still high owing to the complexity of 50-stage TDC. In contrast, the proposed NSQ requires much less TDC quantization levels (ie; $N = 6$), making it more beneficial from the point of power consumption. On the other hand, the proposed quantizer utilizes a NC technique that can achieve the same degree of noise-shaping reported in Dhanasekaran et al.[27]

5 | CONCLUSIONS

In this paper, a time-based NSQ is proposed. The NC technique is utilized in the proposed NSQ to increase the overall noise-shaping order in TCSDMs. Owing to the time-based quantization, using a linearized model for the NSQ becomes more feasible. Using this model, a fully continuous-time implementation of the NSQ is realized. So, the noise-shaping order of a TCSDM is increased up to 2 when the proposed NSQ is utilized. Furthermore, a merged combination of the TDC/DTC is introduced to realize a polyphase time-based sampler. This sampler avoids the need of the challenging multi-bit DAC at the feedback path. The verification of the proposed NSQ is done both in system and circuit levels by using postlayout simulations. Furthermore, a design example of a TCSDM benefited from the proposed NSQ along with the behavioral simulation results is developed to evaluate the effectiveness of the concept.

ORCID

Mohsen Tamaddon http://orcid.org/0000-0002-7358-8437

REFERENCES

1. Lee K, Bonu M, Temes GC. Noise-coupled delta-sigma ADCs. *Elect Letters*. Nov. 2006;42(24):1381-1382.
2. Wang Y, Temes GC. "ΔΣ ADCs with second-order noise-shaping enhancement," in Proc. IEEE Symp. Midwest Circuits and Systems (MWSCAS), pp. 345 - 348, Aug. 2009.
3. Wang Y, Temes GC. Noise-coupled continuous-time delta-sigma ADCs. *Elect. Letters*. Sept. 2009;45(6):302-303.
4. Ding C, Manoli Y and Keller M, "Approaches to the implementation of noise-coupling in continuous-time delta-sigma modulators," in Proc. IEEE Int. Symp. Circuits and Systems (ISCAS), pp. 1047-1050, May. 2013.
5. Brückner T, Kiebler M, Lorenz M. "Calculating transfer functions of CT sigma-delta modulators with arbitrary DAC waveforms," in Proc. IEEE Int. Symp. Circuits and Systems (ISCAS), pp. 1264-1267, May. 2013.

6. Gelb A, Velde WV. *Multiple-Input Describing Functions and Non-Linear System Design*. New York: McGraw-Hill; 1968.
7. Atherthon DP. *Nonlinear Control Eng*. New York: VNR; 1982.
8. Lota J, Al-Janabi M, Kale I. Accurate stability prediction of one-bit higher-order delta-sigma modulators for multiple-sinusoidal inputs. *IET Circuits Devices Sys*. Mar. 2012;6(2):71-78.
9. Rombouts P, Bock MD, Maeyer JD. A describing function study of saturated quantization and its application to the stability analysis of multi-bit sigma delta modulators. *IEEE Trans Circuits Sys Regul Pap*. Jul. 2013;60(7):1740-1752.
10. Weibo L, Orino Y, Shinnosuke H, Minoru KK. Design of a self-oscillating PWM signal generator with a double integration loop. *IEEE Trans Circuits Sys Regul Pap*. Jan. 2013;60(8):2064-2073.
11. Bradley M, Alarcon E, Feely O. Control of limit cycle oscillations in a multiple-sampled digitally controlled buck converter. *Int J Circuit Theory Appl*. published online,. Nov. 2013;
12. Veillette BR, Roberts GW. Delta-sigma oscillators: versatile building blocks. *Int J Circuit Theory Appl*. Sept. 1997;25:407-418.
13. Fei Y. Design techniques for time-mode noise-shaping analog-to-digital converters: a state-of-the-art review. *Analog Integr Circ Sig Process*. Nov. 2014;79:191-206.
14. Tamaddon M, Yavari M. An NTF-enhanced time-based continuous-time sigma-delta modulator. *J Analog Integr Circ Sig Process*. Nov. 2015;85(2):283-297.
15. Hernandez L, Prefasi E, Pun E, Paton S. A 1.2-MHz 10-bit continuous-time sigma-delta ADC using a time encoding quantizer. *IEEE Trans Circuits Syst Express Briefs*. Jan. 2009;56(1):16-20.
16. Pakniat H, Yavari M. A time-domain noise-coupling technique for continuous-time sigma-delta modulators. *Analog Integr Circ Sig Process*. Nov. 2013;78:439-452.
17. Vuyst BD, Rombouts P. A 5-MHz 11-bit self oscillating ΣΔ modulator with a delay-based phase shifter in 0.025 mm^2. *IEEE J Solid State Circuits*. Aug. 2011;46(8):1919-1927.
18. Ouzounov S, Hegt H, van Roermund A. Sigma-delta modulators operating at a limit cycle. *IEEE Trans Circ Syst Express Briefs*. May 2006;53(5):399-403.
19. Ouzounov S, Roza E, Hegt JA. Analysis and design of high-performance asynchronous sigma-delta modulators with a binary quantizer. *IEEE J Solid State Circuits*. Mar. 2006;41(3):588-596.
20. Tamaddon M, Yavari M. A wideband time-based continuous-time sigma-delta modulator with 2nd order noise-coupling based on passive elements. *Int J Circuit Theory Appl*. Mar. 2016;44(3):759-779.
21. Tamaddon M, Yavari M. High performance time-based continuous-time sigma-delta modulators using a single-opamp resonator and a noise-shaped quantizer. *Microelectron J*. Oct. 2016;56(3):110-121.
22. Babaie-Fishani A, Rombouts P. Analytical expressions for the distortion of asynchronous sigma-delta modulators. *IEEE Trans Circ Syst Express Briefs*. Aug. 2013;60(8):472-476.
23. Daniels J, Dehaene W, Steyaert M, Wiesbauer A. A/D conversion using asynchronous ΣΔ modulation and time-to digital conversion. *IEEE Trans Circ Sys Regul Pap*. Sept. 2010;57(9):2404-2412.
24. Colodro F, Torralba A. Spectral analysis of pulsewidth-modulated sampled signals. *IEEE Trans Circuits Syst-II*. Aug. 2010;57(8):622-626.
25. Ortmanns M, Gerfers F. *Continuous-Time Sigma-Delta A/D Conversion*. Springer; 2005.
26. Ashry A, Aboushady H. Fast and accurate jitter simulation technique for continuous-time ΣΔ modulators. *Electron Lett*. Aug. 2009;45(24):1218-1219.
27. Dhanasekaran V, Gambhir M, Elsayed MM, et al. A continuous-time multi-bit ΔΣ ADC using time domain quantizer and feedback element. *IEEE J Solid State Circuits*. March 2011;46(3):639-650.
28. Prefasi E, Paton S, Hernandez L. A 7 mW 20 MHz BW time-encoding oversampling converter implemented in a 0.08 mm 65 nm CMOS circuit. *IEEE J Solid State Circuits*. Jul. 2011;46(7):1562-1574.
29. Hong J-H, Chen Z-Y. "A low-power 10MHz bandwidth continuous-time ΣΔ ADC with Gm-C filter," in Proc. IEEE Int. Symp. Midwest Circuits and Systems (MWSCAS), pp. 853-856, Aug. 2014.

How to cite this article: Tamaddon M, Yavari M. An oscillatory noise-shaped quantizer for time-based continuous-time sigma-delta modulators. *Int J Circ Theor Appl*. 2018;46:384–400. https://doi.org/10.1002/cta.2422